Journal of Physics: Conference Series **154** (2009) 012030 doi:10.1088/1742-6596/154/1/012030

A High Sensitivity Heterodyne Interferometer as a Possible Optical Readout for the LISA Gravitational Reference Sensor and its Application to Technology Verification

Martin Gohlke[1,2], Thilo Schuldt[2,3], Dennis Weise[1], Ulrich Johann[1], Achim Peters[2] and Claus Braxmaier[1,3]

[1] EADS Astrium, Claude-Dornier-Straße, 88039 Friedrichshafen, Germany
[2] Humboldt-Universität zu Berlin, Hausvogteiplatz 5-7, 10117 Berlin, Germany
[3] Hochschule für Technik, Wirtschaft & Gestaltung, Brauneggerstr. 55, 78462 Konstanz, Germany

E-mail: martin.gohlke@astrium.eads.net

Abstract. The space-based gravitational wave detector LISA (Laser Interferometer Space Antenna) utilizes a high performance position sensor in order to measure the translation and tilt of the free flying proof mass with respect to the optical bench. Depending on the LISA optical bench design, this position sensor must have up to pm/$\sqrt{\text{Hz}}$ sensitivity for the translation measurement and up to nrad/$\sqrt{\text{Hz}}$ sensitivity for the tilt measurement. We developed a heterodyne interferometer, combined with differential wavefront sensing, for the tilt measurement. The interferometer design exhibits maximum symmetry where measurement and reference arm have the same frequency and polarization and the same optical path-lengths. The interferometer can be set up free of polarizing optical components preventing possible problems with thermal dependencies not suitable for the space environment. We developed a mechanically highly stable and compact setup which is located in a vacuum chamber. We measured initial noise levels below 10 pm/$\sqrt{\text{Hz}}$ (longitudinal measurement) for frequencies above 10 mHz and below 20 nrad/$\sqrt{\text{Hz}}$ (tilt measurement) for frequencies above 1 mHz. This setup can also be used for other applications, for example the measurement of the coefficient of thermal expansion (CTE) of structural materials, such as carbon fiber reinforced plastic (CFRP).

1. Introduction

In the LISA concept, the detector should be sensitive enough to detect gravitational waves with induced strains of amplitude $h = \Delta l/l \sim 10^{-23}$. Therefore, it is necessary to measure the relative distance between the three spacecraft with an accuracy of a few picometers. But not only gravitational waves will change the distance. External disturbances like solar radiation pressure or solar wind will change the position of the spacecraft and thereby might affect the interferometer signals caused by gravitational waves. Therefore, a free-flying proof mass – as part of the gravitational reference sensor (GRS) – inside the satellite is taken as reference for a purely gravitational orbit. As the external disturbances only act on the surface of the satellite, the distance between proof mass and its housing (which is rigidly connected to the satellite) is changing. In case of a drag-free controlled satellite (drag-free attitude control system, DFACS),

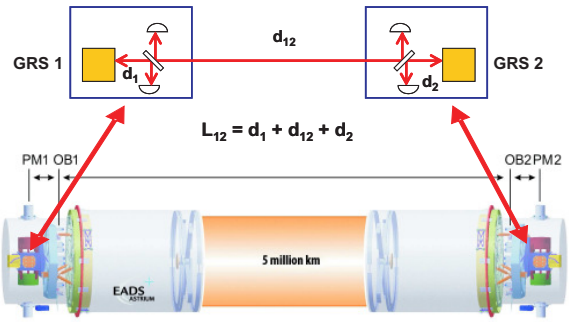

Figure 1. Schematic of the strap-down-architecture. The distance measurement is split into two local, from proof mass (PM) to the optical bench (OB), and one long distance measurement.

any change of the proof mass position is measured and the satellite is controlled in such a way that it is centered around the proof mass at any time, canceling all non-gravitational forces acting on the spacecraft. The proof mass also acts as the end mirror of the interferometer arms.

In the so-called strap-down-architecture (cf. Fig. 1 and [1]) each interferometric measurement of the distance between two satellites is split into three independent measurement: (i) the distance between the proof mass and the optical bench on the first satellite, (ii) the distance between the optical benches aboard the two satellites, and (iii) the distance between the optical bench on the second satellite and its proof mass. The proof mass position sensor is part of the so-called science interferometer and must fulfill requirements of $1\,\mathrm{pm}/\sqrt{\mathrm{Hz}}$ (for frequencies above 2.8 mHz with an f^{-2} relaxation down to $30\,\mu$Hz) for the translation measurement and at least $20\,\mathrm{nrad}/\sqrt{\mathrm{Hz}}$ for the tilt measurement (for frequencies above 0.1 mHz with an f^{-1} relaxation down to $30\,\mu$Hz, DFACS requirements).

These requirements necessitate an optical readout (ORO) of the proof mass position utilizing laser interferometry. Our interferometer concept represents a possible ORO.

2. Interferometer Setup

Our experimental setup is based on a highly symmetric design and represents a heterodyne interferometer with spatially separated beams [2–5]. Reference and measurement beams of the interferometer have the same frequency and polarization. Also, their optical pathlengths (especially inside optical components) are similar. Schematics of our interferometer setup are shown in Figs. 2 and 3, and a photograph in Fig. 4. The phase $\phi(t)$ between the signals on measurement and reference photodiode is proportional to the displacement Δl of the measurement mirror:

$$\phi(t) = \frac{4\pi n}{\lambda} \cdot \Delta l(t)\,, \tag{1}$$

where λ is the vacuum wavelength of the light and n the refractive index of the medium the light is traveling in.

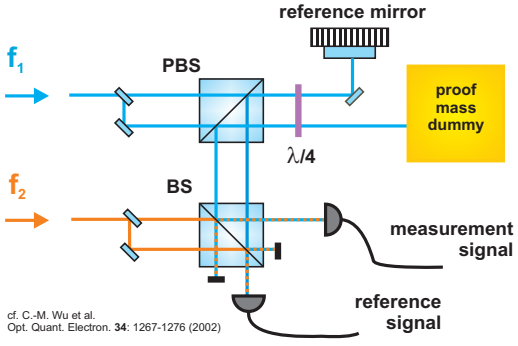

Figure 2. Schematic of the heterodyne interferometer (BS: beamsplitter; PBS: polarizing beamsplitter). The signal at the photodiodes are given by $I_{meas} \sim AB \cdot \cos(\Delta\omega t - \phi(t))$ and $I_{ref} \sim AB \cdot \cos(\Delta\omega t)$. Here, A and B denote the amplitudes of the laser, f_1 and f_2 the frequencies and $\Delta\omega = 2\pi|f_1 - f_2|$.

For in-quadrature measurement, the two signals

$$S_1 = \frac{1}{2} AB \cos\phi(t) \quad \text{and} \quad S_2 = \frac{1}{2} AB \sin\phi(t) \tag{2}$$

are generated, where the phase measurement is obtained by

$$\phi(t) = \tan^{-1} \frac{S_2}{S_1} \,. \tag{3}$$

In order to measure the tilt of the proof mass, the method of Differential Wavefront Sensing (DWS) [6] is implemented. Therefore, we use quadrant photodiodes and the phase difference between opposing halves is measured.

The interferometer setup can be subdivided into two parts: (i) the optical setup for frequency generation, and (ii) the interferometer board. The optics for frequency generation are placed on an optical table using standard optical components. The interferometer board is placed inside a vacuum chamber operated at pressures below 10^{-3} mbar. For mechanical stability and compactness, purpose-built optical component mounts with a beam-height of 2 cm are used.

2.1. Heterodyne Frequency Generation

An NPRO-type (non-planar ring-oscillator) Nd:YAG laser at a wavelength of 1064 nm is used as light source. Part of its output power is split and shifted in frequency by use of two acousto-optic modulators (AOMs). The AOMs are working at a frequency of 79.99 MHz and 80.00 MHz, respectively, resulting in a heterodyne frequency of 10 kHz. The two laser beams are fiber-coupled and sent to the interferometer inside the vacuum chamber via optical single mode fibers. The RF-signals driving the AOMs are generated by use of two phase-locked direct digital synthesizers (DDS).

2.2. Interferometer Setup

The 300mm × 440mm × 40mm interferometer board is made of cast aluminum which offers low internal stresses and therefore reduced long-term drifts of the material. The two frequencies are fiber-coupled to the interferometer board. Polarizers at the fiber inputs and outputs ensure a proper and clean polarization. The optical power of each beam is ∼ 2.5 mW at the fiber output, this is equivalent to 100μW on the proof mass. Both beams are split at a wedged glass plate, the front side reflections are used in the interferometer while the back side reflections are sent to two monitor photodiodes (PD1 and PD2 in Fig. 3). Their signals are taken for intensity stabilization of the laser beams after fiber outcoupling. The amplitudes of the RF signals driving the AOMs are used for actuation of the light intensities. The beams transmitted at the glass

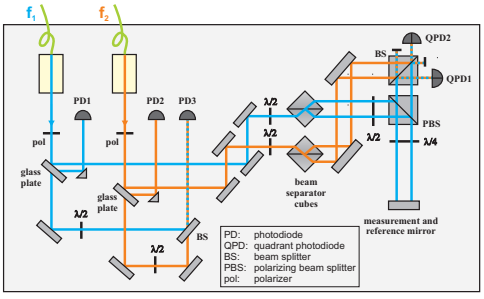

Figure 3. Schematic of the heterodyne interferometer.

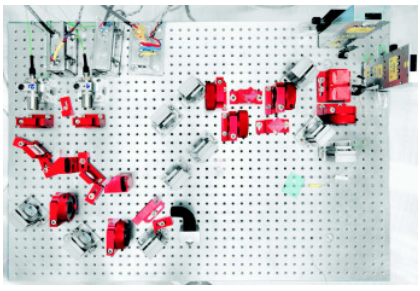

Figure 4. Picture of the interferometer inside the vacuum chamber.

plates are superimposed on a third photodiode (PD3 in Fig. 3). The generated heterodyne signal is phase-locked to a 10 kHz signal which is obtained by mixing the DDS output signals. The signal at the photodiode corresponds to an interferometer signal, where the splitting in measurement and reference beam takes place at the beamsplitter before the AOMs outside the vacuum chamber. Therefore, it contains all differential phase effects caused by the fibers and the AOMs. A piezoelectric actuation of one mirror in one arm of the interferometer outside the vacuum chamber is used for actuation of the feedback loop. The two beams used for the interferometer are both split into two parallel output beams. A symmetric beamsplitter is used providing the same optical path-lengths inside the component. Also, ghost reflections of the input beams are not reflected back in direction of the input beam.

The beams with frequency f_1 are representing measurement and reference beams of the interferometer, the beams with frequency f_2 are used for generating heterodyne signals at the photodiodes. The beams with frequency f_1 are first reflected by a polarizing beamsplitter (PBS) towards the measurement and reference mirror, which in our experiment is realized by one fixed mirror. After passing twice a quarter waveplate ($\sim \lambda/2$), both beams are transmitted at the PBS and superimposed with the beams with frequency f_2 at a (non-polarizing) beamsplitter (BS). Two quadrant photodiodes (QPD1 and QPD2 in Fig. 3) measure the heterodyne signals. Their sum signals are taken for translation measurement, and the signals of opposing halves for tilt measurement.

2.3. Digital Phase Measurement

The signals of the quadrant photodiode are first pre-amplified inside the vacuum chamber. The sum signals and the signals for differential wavefront sensing are generated and amplified outside the vacuum chamber by use of analog electronics. All signals are anti-aliasing filtered by use of a 6^{th} order Bessel filter (corner frequency: 20 kHz). The signals are then simultaneously digitized by a National Instruments field programmable gate array (FPGA) computer board at a frequency of 160 kHz and with a 16 bit resolution. The FPGA board is programmed by LabVIEW. A digital phasemeter is implemented where the corresponding input signals to the FPGA board are multiplied and low-pass filtered. For in-quadrature measurement, the signals phase-shifted by 90° are generated. The data is reduced by a factor of 8000 and transferred to a LabVIEW host program which carries out the calculation as given in Equation (3). The program also monitors phasejumps by π and therefore offers a dynamic range not limited by $\lambda/2$ in mirror translation.

3. Measured Noise Performance

We performed a noise measurement where the measurement and the reference mirror are represented by the same fixed mirror (cf. Fig. 3). The power spectrum density (PSD) of the translation measurement is shown in Fig. 5, the PSD of the corresponding tilt measurement in Fig. 6. The peak near 3 Hz was caused by a missing synchronization of the FPGA clock and the DDS. It is removed in later measurements.

In translation measurements (cf. Fig. 5), noise level below $1\,\text{nm}/\sqrt{\text{Hz}}$ for frequencies above 0.1 mHz and below $10\,\text{pm}/\sqrt{\text{Hz}}$ for frequencies above 10 mHz were obtained. In tilt measurements (cf. Fig.6) the noise level is below $1\,\mu\text{rad}/\sqrt{\text{Hz}}$ for frequencies above 0.1 mHz and below $10\,\text{nrad}/\sqrt{\text{Hz}}$ for frequencies above 10 mHz.

4. Applications

The interferometer setup as described above is a highly sensitive measurement system which can be used to investigate other key aspects in the LISA context. For example:

- determine the coefficient of thermal expansion of ultra-stable structural materials, e.g. carbon fiber reinforced plastic (CFRP),

- testing the noise performance and linearity of various LISA mechanisms, e.g. the actuator of the in-field pointing mechanism as well as the mechanism itself, and
- investigate the quality of mirror surfaces in the pm-range.

Dilatometry
Based on the above presented setup we developed a highly sensitive dilatometer for characterizing the dimensional stability of ultra-stable materials. The principle of the dilatometer is shown in Fig.7. We are changing the temperature of the tube to be tested via radiative heating/cooling and measure the linear expansion with our interferometer with sub-nm resolution. The CTE is given as:

$$CTE = \frac{1}{\Delta T}\frac{\Delta L}{L} \ [K^{-1}]\,. \tag{4}$$

Measurement and reference mirrors are placed at the top and at the bottom inside a tube made by the material under investigation (cf. Fig. 7). The mirror mounts are specifically designed in order not to influence the CTE measurement. Therefore, the reflective surface of each mirror is in the same plane as the clamping points of the mirror mount inside the tube. We also developed a test tube support and a heating/cooling system. For measurement, a sine thermal cycling with a period up to several hours is applied to the device under test (cf. Fig. 8).

Due to limitations of the vacuum chamber and the interferometer setup, we are restricted to tubes with an inner diameter of 20 mm, an outer diameter of $\sim$ 27 mm and a length of 10 cm. The temperature of the device under test can be varied between 20° C and 60° C.

We first performed a measurement with a CFRP tube with a known CTE of $\sim -6.47 \cdot 10^{-7}\,\mathrm{K}^{-1}$. Our result with the interferometer test facility provided a CTE of $\sim -6.10 \cdot 10^{-7}\,\mathrm{K}^{-1}$. In the next step, we procured a new CFRP tube with a predicted CTE below $-2.5 \cdot 10^{-8}\,\mathrm{K}^{-1}$. We measured a CTE of $\sim -3.6 \cdot 10^{-7}\,\mathrm{K}^{-1}$, which does not agree with the theoretical value [7].

Presently, we and the company are analyzing the manufacturing process as the determination of the CTE includes uncertainties.

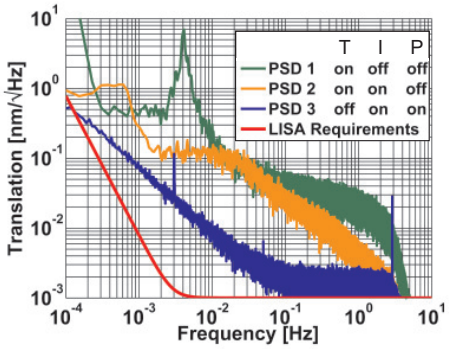

Figure 5. Power spectrum densities (PSD) of the translation noise measurements. The smooth line at the bottom represents the LISA requirements. At the beginning (upper line) with temperature stabilization (T) but without intensity- (I) and phase- (P) stabilization. The lower line represents the current noise performance.

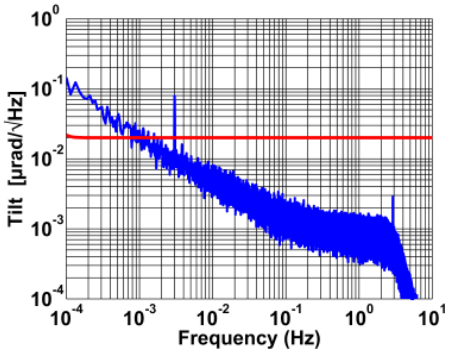

Figure 6. PSD of the tilt noise measurement (T: off, I: on, P: on). The smooth line represents the DFACS requirements. The roll off at 3 Hz is caused by a digital low pass filter in the data acquisition chain.

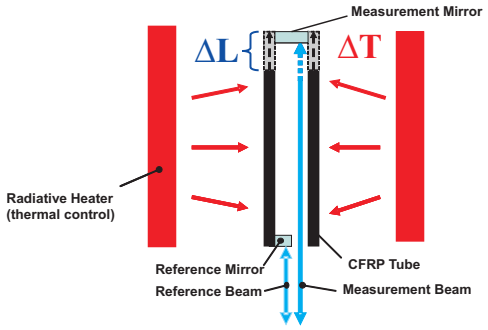

Figure 7. Sketch of our CTE measurement facility.

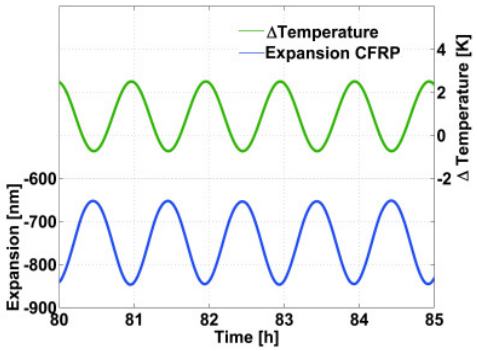

Figure 8. Typical time series of a CTE measurement run. The upper curve represents the cycled temperature of the CFRP probe, the lower curve the measured expansion.

5. Summary and Outlook

We developed a compact setup of a high sensitivity heterodyne interferometer. Noise levels below $10\,\mathrm{pm}/\sqrt{\mathrm{Hz}}$ in translation measurement and below $10\,\mathrm{nrad}/\sqrt{\mathrm{Hz}}$ in tilt measurement – both for frequencies above 10 mHz – were demonstrated in lab experiments. In a current project, the interferometer is adapted as dilatometer for measurement of the thermal expansion of carbon fiber reinforced plastics. Measurements were carried out validating the capability of our setup. In general, the test facility offers the possibility to characterize ultra-stable materials with a CTE down to $10^{-8}\,\mathrm{K}^{-1}$.

Current activities also include the development of a new quasi-monolithic setup using thermally highly stable glass ceramics as breadboard materials in the interferometer.

Acknowledgments

This work is partially supported by the German Aerospace Center (Deutsches Zentrum für Luft- und Raumfahrt e.V.) within the program LISA Performance Engineering (DLR contract number: 50OQ0701).

The authors thank the Albert-Einstein-Institute Hannover, Evgeny Kovalchuk and Klaus Palis from the Humboldt-University Berlin and Hans-Reiner Schulte from EADS Astrium Friedrichshafen for their support and the fruitful discussions.

References

[1] Gath P, Johann U, Schulte H R, Weise D and Ayre M 2006 *Laser Interferometer Space Antenna – 6th International LISA Symposium* (AIP conference proceedings) pp 647–653
[2] Schuldt T, Kraus H J, Weise D, Braxmaier C, Peters A and Johann U 2006 *Proceedings of the* 6th *International Conference on Space Optics (ICSO 2006)*
[3] Schuldt T, Gohlke M, Weise D, Johann U, Peters A and Braxmaier C 2007 *Proceedings of SPIE* (6717, Optomechatronic Sensors and Instrumentation III, 67160F)
[4] Schuldt T, Gohlke M, Weise D, Johann U, Peters A and Braxmaier C *International Journal of Optomechatronics* **1**
[5] Wu C, Lin S and Fu J *Opt. Quantum Electron. 12* **34** 1267–1276
[6] Morrison E, Meers B J, Robertson D I and Ward H *Appl. Opt. 22* **33**
[7] Cordero J, Heinrich T, Schuldt T, Gohlke M, Lucarelli S, Weise D, Johann U, Peters A and Braxmaier C 2008 *Proceeding of SPIE* (7018, Advanced optical and mechanical technologies in telescopes and instrumentation)